Scientific Research Publishing

Open Journal of Inorganic Chemistry, 2022, 12, 39-56
https://www.scirp.org/journal/ojic
ISSN Online: 2161-7414
ISSN Print: 2161-7406

Molecular Modeling and Antimicrobial Screening Studies on Some 3-Aminopyridine Transition Metal Complexes

Islam M. I. Moustafa*, Naglaa M. Mohamed, Sahar M. Ibrahim

Chemistry Department, Faculty of Science, Benha University, Benha, Egypt
Email: *Islamshahin84@outlook.com, naglaaali30@yahoo.com, drsaher247@yahoo.com

How to cite this paper: Moustafa, I.M.I., Mohamed, N.M. and Ibrahim, S.M. (2022) Molecular Modeling and Antimicrobial Screening Studies on Some 3-Aminopyridine Transition Metal Complexes. *Open Journal of Inorganic Chemistry*, **12**, 39-56.
https://doi.org/10.4236/ojic.2022.123003

Received: June 19, 2022
Accepted: July 26, 2022
Published: July 29, 2022

Abstract

Seven transition metal complexes of Mn^{2+}, Ni^{2+}, Co^{2+}, Cu^{2+} and Zn^{2+} with 3-aminopyridine (3-APy) as ligand have been synthesized, characterized by different techniques and their antibacterial activities were studied. Molecular modeling calculations were performed using $DMOL^3$ program in materials studio package which is designed for the realization of large scale density functional theory calculation (DFT). The quantum mechanical and chemical reactivity parameters such as chemical hardness, chemical potential, electronegativity, electrophilicity index and Homo-Lumo energy gap were obtained theoretically and were used to understand the biological activity of the prepared compounds. Some complexes were tested for their *in-vitro* cytotoxic activity in human lung cancer cell lines (A-549 cell line), and structure-activity relationships were established. In general, the coordination to Co^{2+} increased the cytotoxicity while the Ni^{2+} complexes show reduced cytotoxic activity compared to the metal-free 3-aminopyridine.

Keywords

3-Aminopyridine, Transition Metal Complexes, Biological, Cytotoxic Activities, Molecular Orbital Calculation, Density Functional Theory

1. Introduction

Pyridine derivatives are very important chemicals with many biological applications. They are known to have moderate-excellent activities towards variety of biological targets varying from microbial diseases to viral organisms and cancerous cells by interacting with enzymes, proteins and DNA [1] [2] [3] [4]. Oxime and hydrazone derivatives of pyridine exhibit high activity against *in-*

fluenza B-Mass virus, HIV and are also used as antidotes against poisoning by organophosphorus compounds [5] [6]. Many metal complexes with pyridine based ligands exhibit high cytotoxicity and have proved to be antitumor agents [7]-[11]. Molecular modeling (MM) is one of the fastest growing fields in science. It may vary from building and visualizing simple molecules in three dimensions (3D) to performing complex computer simulations on large proteins and nanostructures [12]. It is a collection of computer-based techniques for driving, representing and manipulating the structures and reactions of molecules depending on 3D structures. The techniques cover several issues among them computational chemistry, drug design, computational biology, nanostructures, and material science [13]. In recent years, density functional theory (DFT) has become an increasingly useful tool for theoretical studies. The success of DFT is due it is computationally less demanding than wave function based methods with inclusion of electron correlation [14]. In the present work seven Mn^{2+}, Co^{2+}, Ni^{2+}, Cu^{2+} and Zn^{2+}-3-aminopyridine (3-APy) complexes with variable stoichiometric ratios were prepared, characterized and their antibacterial activities were studied. Some complexes were tested for their *in*-vitro cytotoxic activity in human lung cancer cell lines (A-549 cell line), and structure-activity relationships were established. Also, the molecular structure of some selected metal complexes in view of chemical reactivity values such as chemical hardness, chemical potential electronegativity, electrophilicity index and HOMO-LOMO energy gap obtained theoretically were described.

2. Experimental

All reagents used were of the highest quality chemicals and were used without further purification. Aqueous solution of 1.00 mmol of metal salts was added with stirring to an ethanolic solution of 3-aminopyridine ligand with the desired molar ratio. The mixture was refluxed for ≈6 hours then cooled to room temperature, and the solid complexes so formed were filtered off and washed with distilled water followed by ethanol and dried under vacuum. Elemental analysis, spectroscopic studies and cytotoxic activity are as reported in our previous work [15].

2.1. Antimicrobial Screening

The antibacterial activity of some complexes toward some bacterial strains and fungi was evaluated by agar well diffusion method [16] [17]. The activity was evaluated by measuring the diameter of zone of inhibition in mm. A medium with DMF as solvent was used as a negative control whereas media with Ampicillin were screened separately for its standard antibacterial activity.

2.2. Molecular Modeling

The cluster calculations using $DMOL^3$ program [18] in materials studio package [19] which is designed for the realization of large scale density functional theory

calculation (DFT) were performed. DFT semi-core pseudopods calculations (dspp) were performed with the double numerica basis sets plus polarization functional (DNP). The DNP basis sets are of comparable quality to 6 - 31 G Gaussian basis sets [20].

3. Results and Discussion

3.1. Characterization of the Metal Complexes

The as-prepared complexes were characterized by different techniques and are proved to have the following structural formulae:

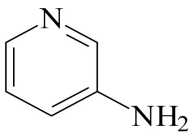

3-aminopyridine (3-APy)

1) $MnBr_2$ ← 3-APy (1:6), $C_{30}H_{36}N_{12}MnBr_2$, M. Wt. 777.09, (% H 4.67, % C 46.33, % N 21.62 and % Mn 7.07)

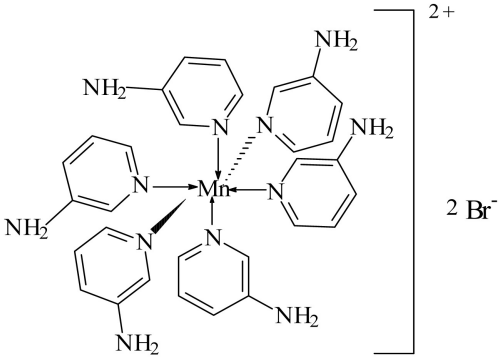

2) $NiCl_2$ ← 3-APy (1:6), $C_{30}H_{36}N_{12}NiCl_2$, M. Wt. 692.19, (% H 5.24, % C 52.01, % N 24.28 and % Ni 8.37)

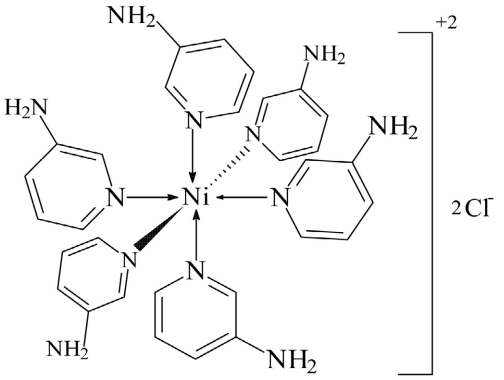

3) $CoCl_2$ ← 3-APy (1:6), $C_{30}H_{36}N_{12}CoCl_2$ M. Wt. 694.54, (% H 5.22, % C 51.88, % N 24.20 and % Co 8.49)

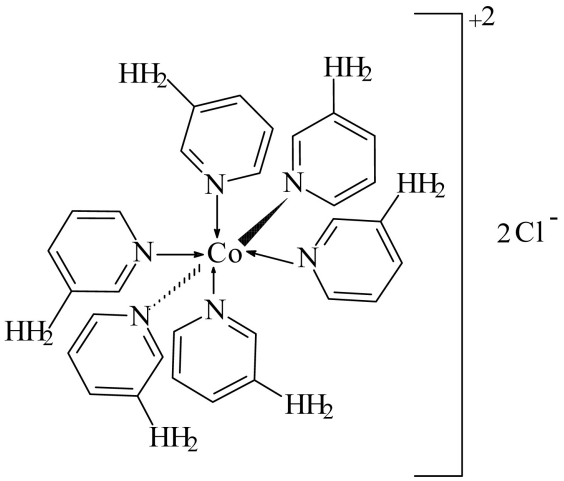

4) $CuCl_2$ ← 3-APy (1:2), $C_{10}H_{16}N_4O_2Cl_2Cu$, M. Wt. 357.00, (% H 4.52, % C 33.61, % N 15.69 and % Cu 17.63)

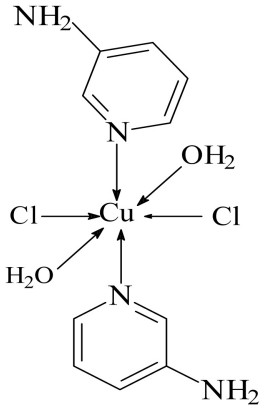

5) $CuCl_2$ ← 3-APy (1:6), $C_{30}H_{36}N_{12}CuCl_2$, M. Wt. 697.19, (% H 5.19, % C 51.54, % N 24.04 and % Cu 9.09)

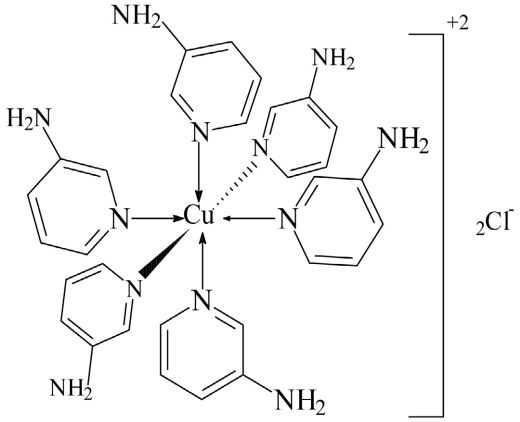

6) $Cu(CH_3COO)_2$ ← 3-APy (1:2), $C_{14}H_{22}N_4O_6Cu$, M. Wt. 405.08, (% H 5.47, % C 41.47, % N 13.83, % O 23.69 and % Cu 15.53)

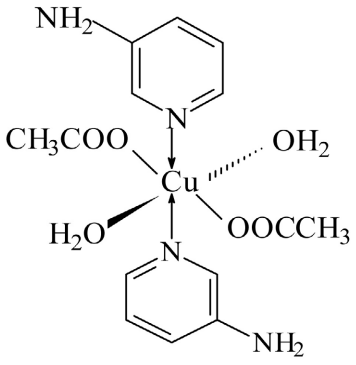

7) $ZnCl_2$ ← 3-APy (1:2), $C_{10}H_{16}N_4O_2Cl_2Zn$, M. Wt. 360.55, (% H 4.50, % C 33.52, % N 15.65, % Zn 17.86)

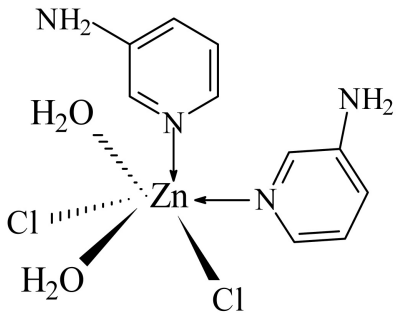

3.2. Thermal Analysis

Up to 800˚C, the prepared metal complexes degrade thermally through, more or less, three main steps. Representative thermogram is shown in Figure 1 and the thermal degradation patterns show that the physically adsorbed and coordinated water molecules are dehydrated from the coordination sphere in two successive steps within the temperature range 80˚C - 220˚C followed by full thermal decomposition at temperature higher than 335˚C leading to metal oxides as final products.

3.3. Infrared Spectra

The IR spectra of the complexes M ← 3-aminopyridine were studied in terms of their molecular structure. The most important band frequencies (cm^{-1}) are cited in Table 1 from which it is found that the spectra exhibit broad band within the range 3400 - 3448 cm^{-1} and weak band within the range 2955 - 3024 cm^{-1} due to the stretching vibrations of OH and NH_2 (V_{OH} and V_{NH2}) groups, respectively. This remarkable broadness and shifting to lower frequencies indicates their contribution in coordination process. This is supported by the appearance of new broad bands within the range 3400 - 3350 cm^{-1} and 574 - 545 cm^{-1} due to the stretching vibrations of coordinated water molecules and the M-O bond, respectively. The stretching vibration of the C=N group ($V_{C=N}$) in the 3-aminopyridine moiety appears at 1545 - 1655 cm^{-1} range while that of the stretching vibration of the C-N group (V_{C-N}) appears at 1516 - 1575 cm^{-1} range. The OH in-plane

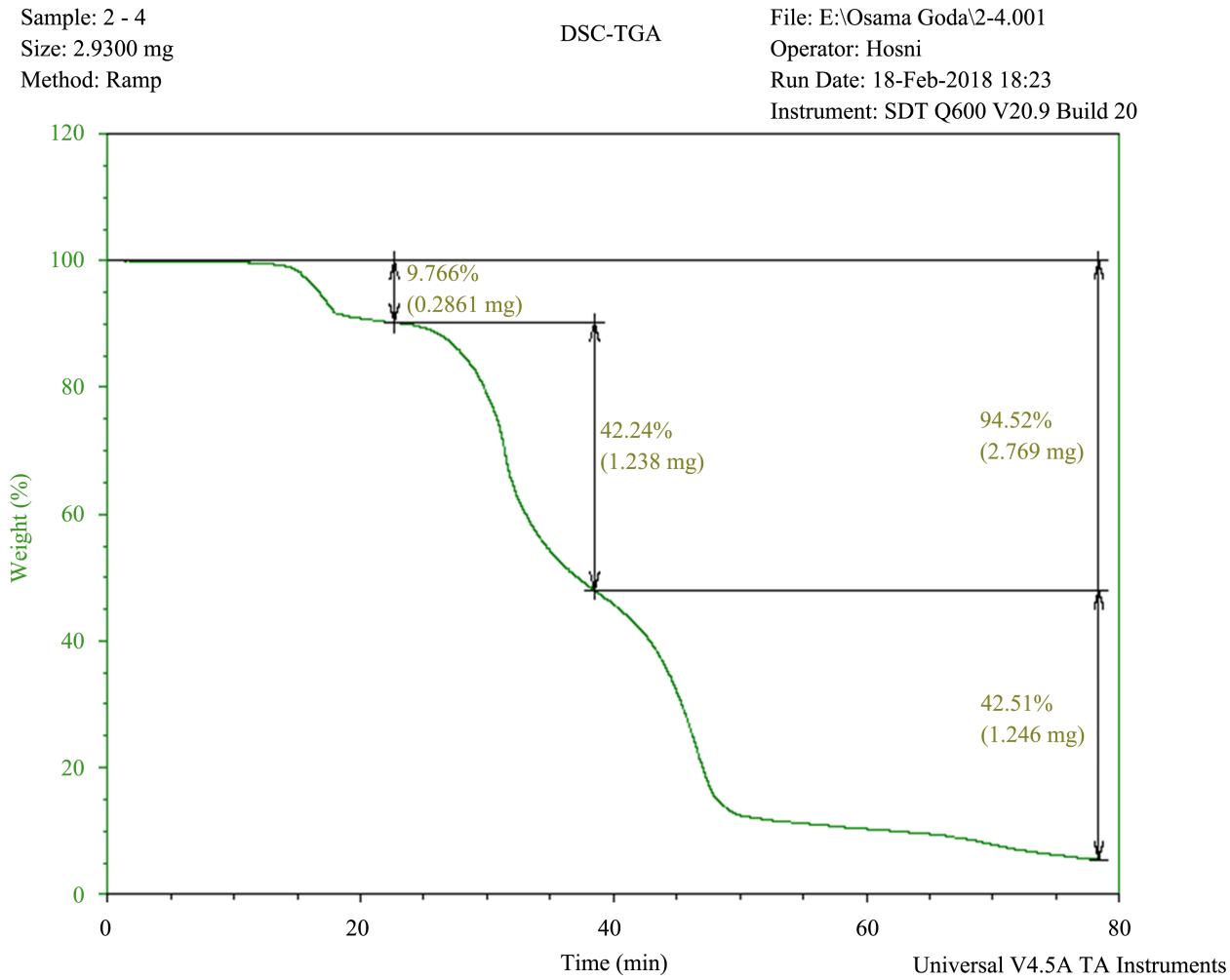

Figure 1. Thermogram of the complex $NiCl_2 \leftarrow$ 3-APy (1:6).

Table 1. IR vibrational frequencies (cm^{-1}) of some function groups of Mn^{2+}, Co^{2+}, Ni^{2+}, Cu^{2+} and Zn^{2+} complexes with 3-aminopyridine.

Complex	V_{OH}	V_{NH2}	$V_{C=N}$	V_{C-N}	δ_{OH}	V_{M-Cl}	V_{M-N}
$MnBr_2 \leftarrow$ 3-APy (1:6)	3400	2960	1653	1525	1101	545	505
$NiCl_2 \leftarrow$ 3-APy (1:6)	3448	2965	1655	1522	1098	525	510
$CoCl_2 \leftarrow$ 3-APy (1:6)	3400	2963	1650	1530	1105	529	508
$CuCl_2 \leftarrow$ 3-APy (1:2)	3435	2955	1645	1525	1105	573	523
$CuCl_2 \leftarrow$ 3-APy (1:6)	3424	3945	1650	1575	1110	553	527
$Cu(Ac)_2 \leftarrow$ 3-APy (1:2)	3403	3024	1651	1516	1021	558	497
$ZnCl_2 \leftarrow$ 3-APy (1:2)	3433	3020	1650	1520	1018	558	483

deformation of the coordinated water molecules gives rise to band within the range 1018 - 1110 cm^{-1}. The out-of-plane deformation of the OH group of the complexes is represented by the strong band within the range 852 - 740 cm^{-1},

while the far infrared region of the spectra of the metal chelates shows new sets of bands within the region 525 - 573 and 483 - 527 cm^{-1} which are due to M-Cl and M-N bonds, respectively.

3.4. Electron Spin Resonance (ESR) Spectra

The X-Band ESR spectra of the powder $CuCl_2 \leftarrow$ 3-APy (1:2) and $Cu(Ac)_2 \leftarrow$ 3-APy (1:2) complexes were recorded at room temperature using DPPH as reference standard (c.f. Figure 2). The ESR exhibits anisotropic spectra with $g_{\perp} > g_{II} > g_e$ ($g_e = 2.0036$ free ion value) characteristic for compressed axial symmetry of the coordination sphere (one coordination axis (z) is significantly shorter than the other two (x, y) with d_{x2-y2} ground state. One unpaired electron in Cu (II) complex with $^2B_{1g}$ as ground state lies in d_{z2} orbital. Analysis of spectra gave the g_{II} and $g_{\perp}$ values as cited in Table 2.

Table 2. ESR spectral parameters for Cu(II) complexes.

Complex	g_{II}	$g_{\perp}$
$Cu(CH_3COO)_2 \leftarrow$ 3-APy (1:2)	**2.15534**	**2.24797**
$CuCl_2 \leftarrow$ 3-APy (1:2)	**2.10094**	**2.16535**

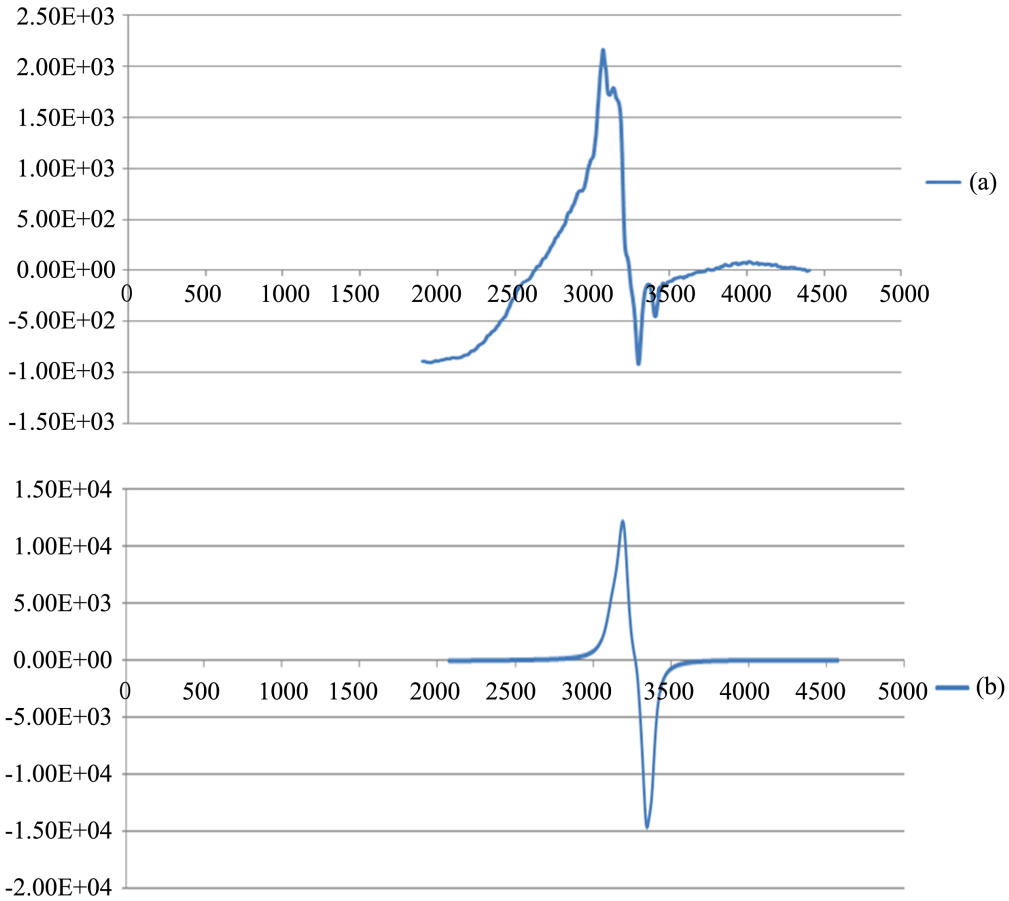

Figure 2. ESR spectra of $Cu(CH_3COO)_2 \leftarrow$ 3-APy (a) and $CuCl_2 \leftarrow$ 3-APy (b).

3.5. Magnetic Moments and Electronic Absorption Spectra

Magnetic moments and electronic spectral data give information about the oxidation state and stereochemistry of the central metal ion in coordination complexes. The data are presented in Table 3.

The magnetic moment of Mn(II) complex is 5.85 BM indicating d^5 high spin (t_{2g}^3 e_g^2) configuration,(spin only value (5.92 BM) while that for Co(II) complex is 5.17 BM indicating d^7 high spin (t_2g^5 eg^2) configuration (spin only value 3.88) which agree with octahedral range 4.3 - 5.2 BM. Ni(II) complexes showed the magnetic moment values of 3.20 BM consistent with their d^8 (t_2g^6 eg^2) octahedral environment. Cu(II) complexes showed magnetic moments of 1.77 BM, slightly higher than the spin-only value (1.73 BM) expected for one unpaired electron d^9 (t_2g^6 eg^3), offering the possibility of octahedral geometry [21]. These geometries are further confirmed by electronic transitions. The Zn (II) complex is observed to be diamagnetic as expected from its electronic configuration**.** The electronic spectral data (measured using Nujol mull technique) are used for assigning the stereochemistry of metal ions in the complexes based on the d-d transitions observed (*c.f.* Table 3).

3.6. Biological Activity

The antimicrobial and antifungal activities of selected complexes were tested against two bacterial; ***Staph. aureus***, ***E. coli*** and two fungi; ***Asper. ocherations***, ***Asper. niger*** species. Standard drug; Ampicillin and DMF solvent control were screened separately for their antibacterial activity. The results and percent activity (*c.f.* Table 4) show that:

1) For antimicrobial activity, the tested complexes show higher activity towards ***Staph. aureus*** than that for ***E. coli***. In the former case, $MnBr_2$ (1:6) has the highest activity followed by $CuCl_2$ (1:6), $CuSO_4$ (1:2), $CuCl_2$ (1:2), $ZnCl_2$ (1:2) and $NiCl_2$ (1:6) while $CoCl_2$ (1:6) has no activity. For ***E. coli***; the activity lies in the order $CuCl_2$ (1:2) > $CuCl_2$ (1:6) > $ZnCl_2$ (1:2) > $MnBr_2$ (1:6) > $CoCl_2$ (1:6) > $NiCl_2$ (1:6) > $CuSO_4$ (1:2).

Table 3. Magnetic moments and spectral data for selected complexes.

Complex	Magnetic moment (B.M)	Electronic absorption spectra (cm^{-1}) Assignment
$MnBr_2$ ← 3-APy (1:6)	5.85	28,260 32,151 $^4T_{2g}(D) \leftarrow {}^6A_{1g}$ $^4T_{1g}(p) \leftarrow {}^6A_{1g}$
$NiCl_2$ ← 3-APy (1:6)	3.20	9105 16,024 26,545 $^3T_{2g}(F) \leftarrow {}^3A_{2g}$ $^3T_{1g}(F) \leftarrow {}^3A_{2g}$ $^3T_{1g}(P) \leftarrow {}^3A_{2g}$
$CoCl_2$ ← 3-APy (1:6)	5.17	9199 16,727 32,786 $^4T_{2g}(F) \leftarrow {}^4T_{1g}$ $^4Ag_2(F) \leftarrow {}^4T_{1g}$ $^4g_1(P) \leftarrow {}^4T_{1g}$
$CuCl_2$ ← 3-APy (1:2)	1.77	1072 28,011 2A1g ← 2B1g 2B2g ← 2B1g
$ZnCl_2$ ← 3-APy (1:2)	Diamagnetic	CT transitions

Table 4. Antibacterial and antifungal activities of some complexes in terms of inhibition zone diameter (mm) and % activity index (% Ac. Ind.).

Complex	*Staph. aureus*		*E. coli*		*Asper. ocherations*		*Asper. niger*	
	Inh. zone "mm"	% Ac. Ind.	Inh. zone "mm"	% Ac. Ind.	Inh. zone "mm"	% Ac. Ind.	Inh. zone "mm"	% Ac. Ind.
Ampicillin	10.33	100	18.33	100	19.67	100	19.67	100
3-APy	9.5	92.00	14.4	78.56	17.0	86.43	17.2	87.44
$MnBr_2$ + 3-Am "1:6"	12.00	116.12	16.33	89.09	13.33	67.70	0	0
$NiCL_2$ + 3-Am "1:6"	10.00	96.77	11.67	63.64	13.67	69.49	0	0
$CoCL_2$ + 3-Am "1:6"	0	0	14.67	80	20.33	103.38	0	0
$CuCL_2$ + 3-Am "1:2"	10.67	103.22	19.67	107.27	18.67	94.92	10.33	52.54
$Cu(Ac)_2$ ← 3-APy "1:2"	11.33	109.68	9.67	52.73	20.00	101.69	11	55.93
$CuCL_2$ + 3-Am "1:6"	11.70	113.26	19.5	106.38	18.70	95.07	10.8	54.91
$ZnCL_2$ + 3-Am "1:2"	11.2	108.42	17.2	93.84	17.4	88.46	11.5	58.46

2) For antifungal activities, the tested complexes have very high activity towards ***Asper. ocherations*** compared to that for ***Asper. niger*** where it was found that for ***Asper. ocherations*** $CoCl_2$ (1:6) and $Cu(Ac)_2$ (1:2) have higher activity than ampicillin and other complexes showed very high activities. On the other hand, the tested complexes showed nearly no activities towards ***Asper. niger*** except for the complexes $CuCl_2$ (1:2 and 1:6), $Cu(Ac)_2$ (1:2) and $ZnCl_2$ (1:2).

Inspection of the data cited above shows that, as a general trend, the activity of the complexes is higher than that of the free ligand. The increase in activity is simply due to the fact that chelation process reduces the polarity of the ligand due to partial sharing of its negative charge with metal ion favoring transportation of the complexes across the lipid layer of the cell membrane [22] [23]. This is in accordance with the calculated quantum chemical analysis data, gathered from molecular modeling studies (as will be shown later in Section 3.2.1), where it is found that complexes show a decrease in the HOMO-LOMO energy gap (ΔE) and increase in each of electronegativity (χ), chemical potential (μ) and electrophilicity (ω). This result suggests the very diffusion of the complexes into the bacterial membrane favoring the antimicrobial activity.

3.7. Antitumor Activity

The cytotoxic activities of some selected complexes were tested against ***Lung carcinoma cells*** **A-549 cell line** and compared to that of Vinblastine as a standard drug. The 50% inhibitory concentration (IC_{50}) was estimated from graphic plots of the relation between surviving cells and complex concentration. The lethal concentrations (IC_{50}) values with a brief comment on the data are listed in Table 5.

Table 5. The lethal concentrations (IC_{50}) values and brief comment on the data of the complexes against Lung carcinoma under the experimental conditions.

Complex	IC_{50} (μg/ml), comment
Vinblastine	4.6 μg/ml
{$ZnCl_2$ & 3-amino "1:2"}	*Moderate Inhibitory activity with IC_{50} = 188 ± 4.3 μg/ml.*
{$NiCl_2$ & 3-amino "1:6"}	*Weak Inhibitory activity with IC_{50} = 354 ± 8.7 μg/ml.*
{$CoCl_2$ & 3-amino "1:6"}	*High Inhibitory activity with IC_{50} = 81.6 ± 2.4 μg/ml.*
{$CuCl_2$ & 3-amino "1:2"}	*High Inhibitory activity with IC_{50} = 108 ± 2.7 μg/ml.*

From the data cited in the Table, it is clear that Co(II) and Cu(II) complexes have high activity toward lung carcinoma cell with a low IC_{50} value (81.6 ± 2.4 and 108. ± 2.7 μg/ml, respectively) while Zn(II) complex showed moderate activity. On the other hand, Ni(II) complex showed weak activity against the tested cell line (IC_{50} value 354 ± 8.7 μg/ml).

3.8. Molecular Orbital Calculations

3.8.1. Molecular Modeling

The molecular modeling, the total density function, deformation density function and frontier orbital energy (the HOMOs and LUMOs) for the ligand 3-aminopyridine and its Ni^{2+}, Cu^{2+} and Zn^{2+} complexes were determined using DFT method. The quantum chemical parameters of the studied complexes were calculated as given in **Table 6**.

The HOMOs and LUMOs are known as Frontier molecular orbitals (FMOs), which play an important role for evaluating molecular chemical stability, and hardness-softness of the molecule [24]. The energy gap, ΔE ($E_{HOMO} - E_{LOMO}$), represents the chemical reactivity of compounds, (system of lower value of ΔE is more reactive). As depicted in **Table 6**, the free ligand (3-APy) has the largest energy gap (2.889 eV) which decreases in case of complex species indicating their stability. Another global reactivity descriptor electrophilicity index (ω) which describes the electron accepting ability of the systems quite similar to hardness and chemical potential. High values of electrophilicity index increases electron accepting abilities of the molecules. The latter values increase in case of complex species indicating the increase in their electron accepting abilities. The direction of the charge transfer is completely determined by the electronic chemical potential (μ) of the molecule because an electrophile is a chemical species capable of accepting electrons from the environment and its energy must decrease upon accepting electronic charge. Electronegativity (χ), chemical potential (μ), global hardness (η), global softness (σ), additional electronic charge (ΔN_{max}) and global electrophilicity index (ω) [25] [26] were calculated and listed in **Table 6**:

$$\chi = -1/2\left(E_{LUMO} + E_{HOMO}\right), \quad \mu = -\chi = 1/2\left(E_{LUMO} + E_{HOMO}\right)$$

$$\eta = 1/2\left(E_{LUMO} - E_{HOMO}\right), \quad \Delta N_{max} = -\mu/\eta, \quad \omega = \mu^2/2\eta, \quad \sigma = 1/\eta$$

Some energetic properties of ligand 3-APy and its complexes were calculated by DFT method and are given in **Table 7**.

Table 6. The quantum chemical parameters of the studied complexes of ligand 3-APy.

Comp.	HOMO (ev)	LUMO (ev)	ΔE	H	Σ	X	μ	Ω	ΔNmax
3-APy	−4.559	−1.670	2.889	1.444	0.692	−3.115	3.12	3.358	2.156
3-APy-$NiCl_2$ (1:6)	−1.629	−1.165	0.464	0.232	4.310	−1.397	1.40	4.206	6.022
3-APy-Cu Cl_2 (1:2)	−4.032	−3.397	0.635	0.318	3.149	−3.715	3.72	21.728	11.699
3-APy-$Cu(Ac)_2$ (1:2)	−4.377	−3.883	0.494	0.247	4.048	−4.130	4.13	34.528	16.721
3-APy-Zn Cl_2 (1:2)	−3.513	−3.362	0.151	0.076	13.245	−3.438	3.44	78.254	45.529

Table 7. Some energetic properties of ligand 3-APy and its complexes calculated by DFT-method.

Comp.	Energy (Kcal/mol)						Binding energy $\times 10^3$
	Sum of atomic energies $\times 10^6$	Kinetic energy $\times 10^3$	Electrostatic energy $\times 10^3$	Exchange-correlation energy $\times 10^3$	Spin polarization energy $\times 10^3$	Total energy $\times 10^6$	
3-APy	−1.892	−1.979	−0.4845	0.506	0.548	−1.906	−1.410
3-APy-$NiCl_2$ (1:6)	−1.257	−4.345	−10.891	3.782	2.987	−1.265	−8.471
3-APy-Cu Cl_2 (1:2)	−1.191	−2.369	−3.48	1.244	1.211	−1.194	−3.397
3-APy-$Cu(Ac)_2$ (1:2)	−1.191	−2.369	−3.48	1.244	1.211	−1.194	−3.397
3-APy-$ZnCl_2$ (1:2)	−1.211	−1.409	−4.435	1.273	1.205	−1.214	−3.364

3.8.2. Geometry Optimization with DFT Method

The molecular structures, atomic numbering, representative bond angles along with the total density of the studied complexes are shown in Structures 1-4. The total density and spin density of the complex are shown in Figures 3-10. From the data given, it is clearly found that the bond angles of the free ligand are altered somewhat upon coordination.

1) The complex $NiCl_2$: 3-APy (1:6)

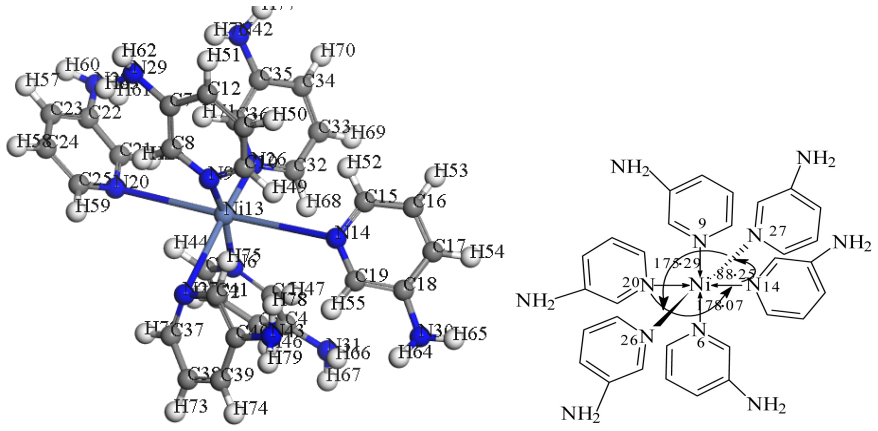

Structure 1. Structure and selected bond angles of the complex $NiCl_2$: 3-APy (1:6).

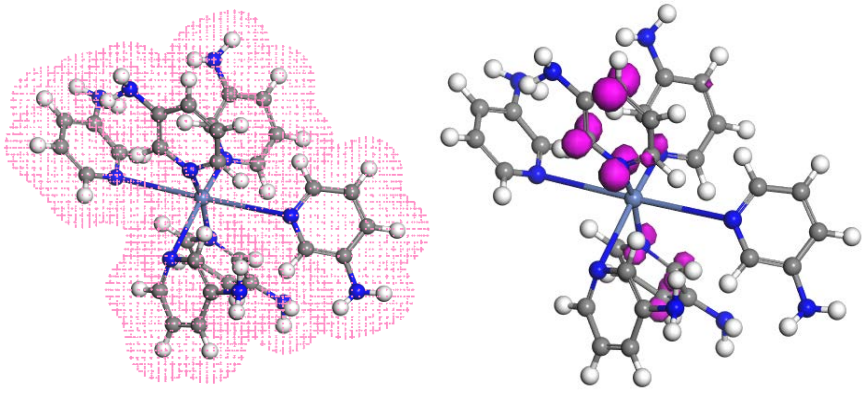

Figure 3. Total density and spin density using DFT method of the complex Ni: 3-APy (1:6).

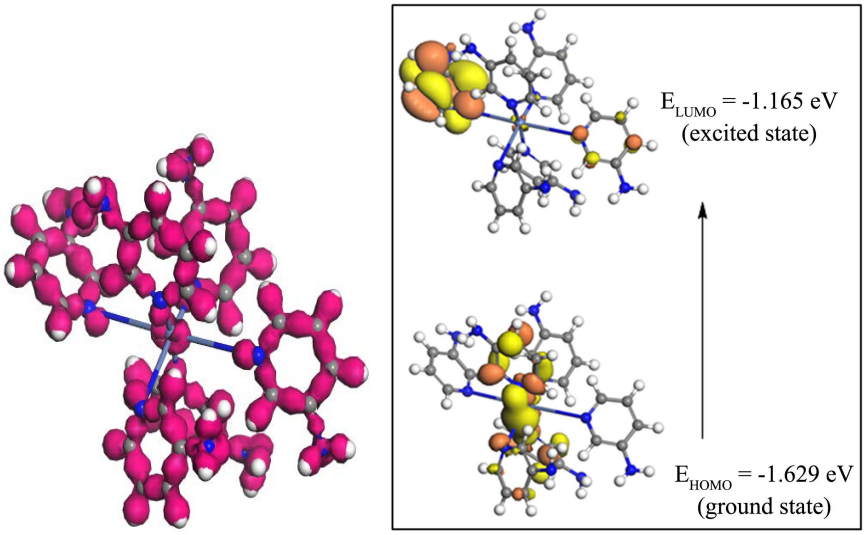

Figure 4. Deformation density and 3D plots frontier orbital energies using DFT method for the complex Ni: 3-APy (1:6).

2) The complex $CuCl_2$: 3-APy (1:2)

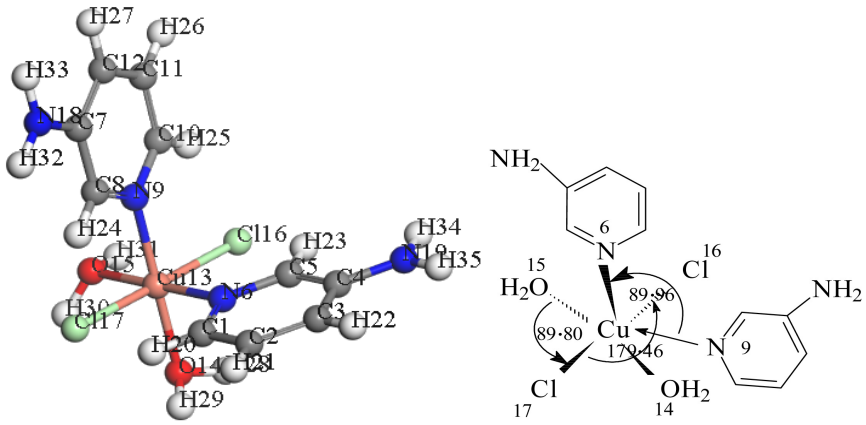

Structure 2. Molecular modeling, structure and selected bond angles of the complex $CuCl_2$: 3-APy (1:2).

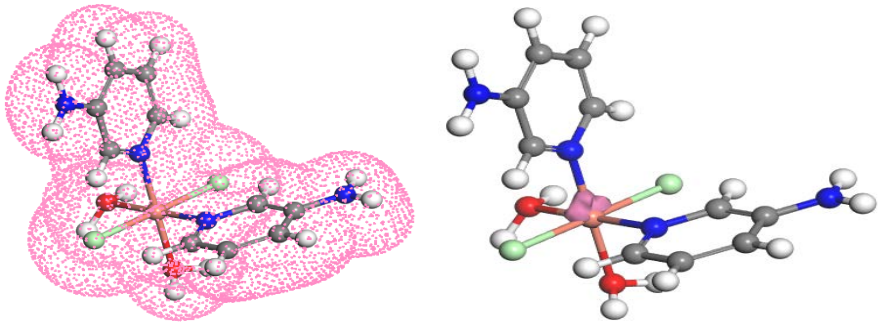

Figure 5. Total density and spin density using DFT method of the complex $CuCl_2$: 3-3-APy (1:2).

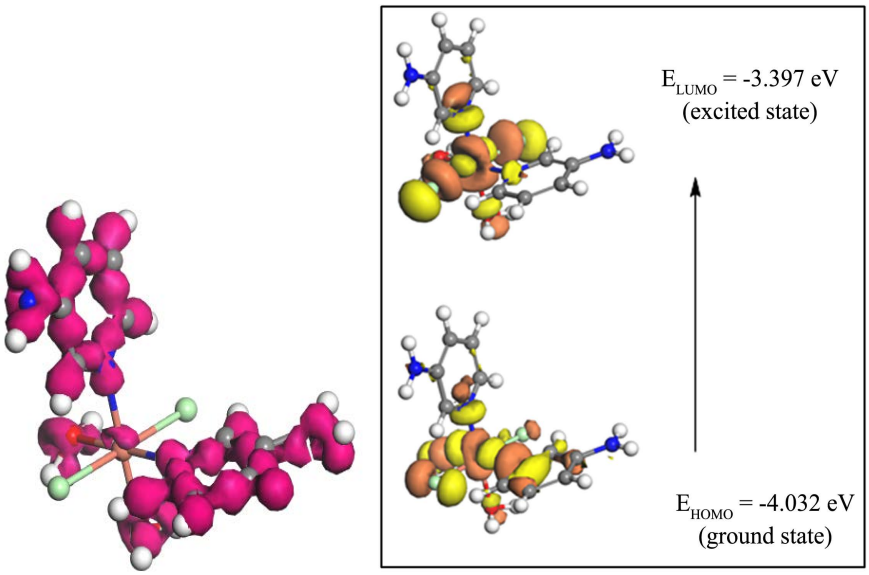

Figure 6. Deformation density and 3D plots frontier orbital energies using DFT method for the complex $CuCl_2$: 3-3-APy (1:2).

3) The complex $Cu(Ac)_2$: 3-APy (1:2)

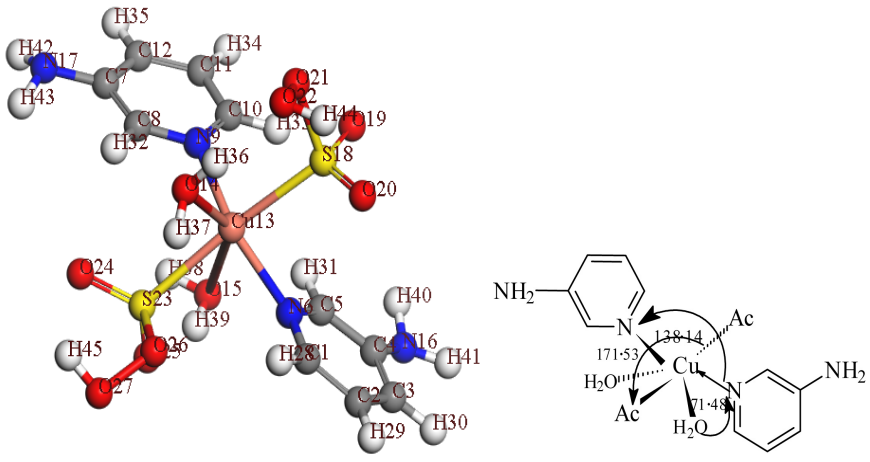

Structure 3. Molecular modeling, structure and selected bond angles of the complex $Cu(Ac)_2$: 3-APy (1:2).

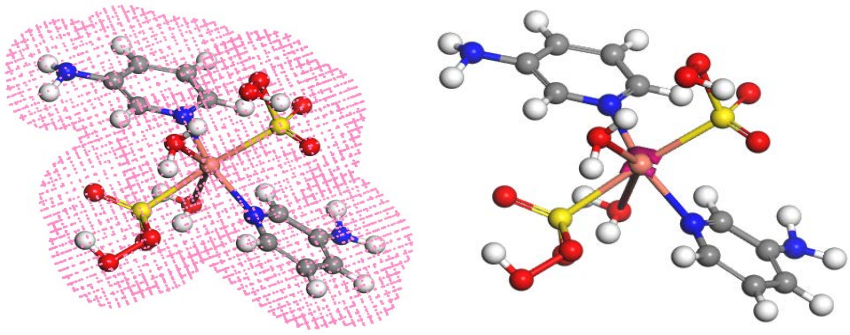

Figure 7. Total density and spin density using DFT method for the complex $Cu(Ac)_2$: 3-APy (1:2).

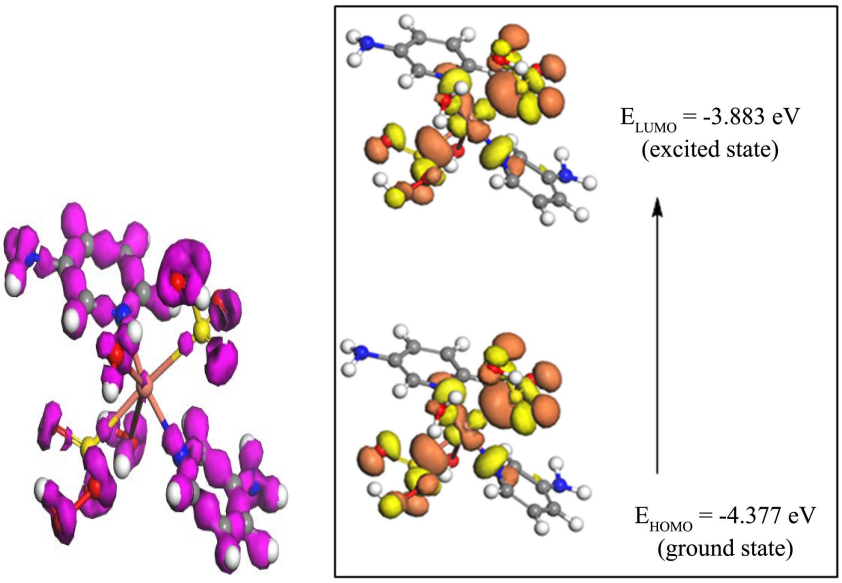

Figure 8. Deformation density using and 3D plots frontier orbital energies using DFT method for The complex $Cu(Ac)_2$: 3-APy (1:2).

4) The complex $ZnCl_2$: 3-APy (1:2)

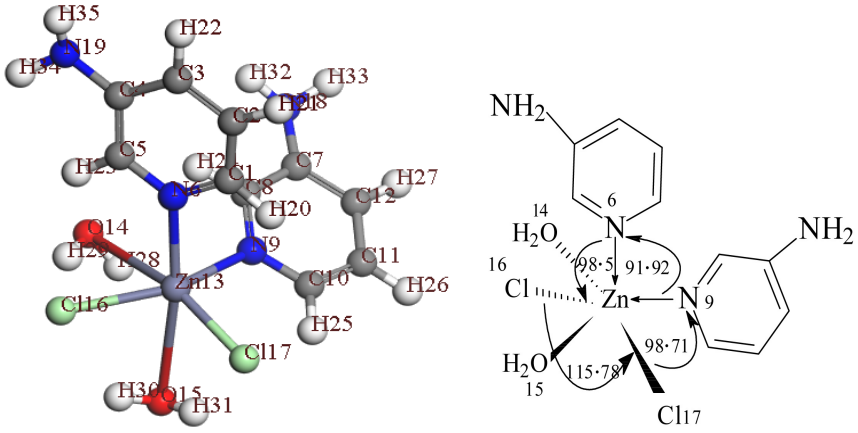

Structure 4. Molecular modeling, structure and selected bond angles of the complex $ZnCl_2$: 3-APy (1:2).

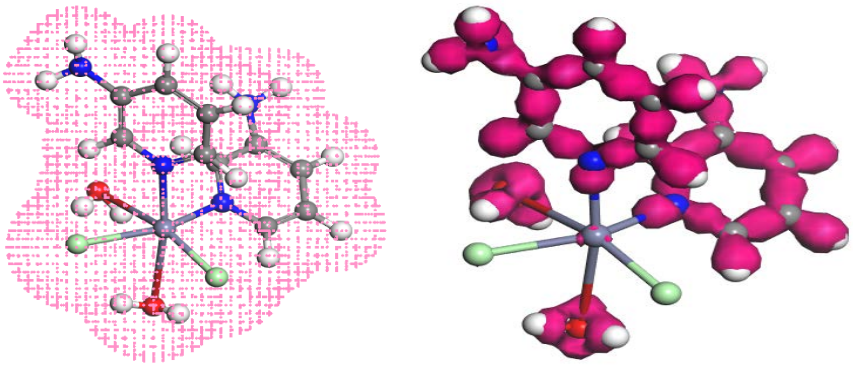

Figure 9. Total density and deformation density using DFT method the complex $ZnCl_2$ ← 3-APy (1:2).

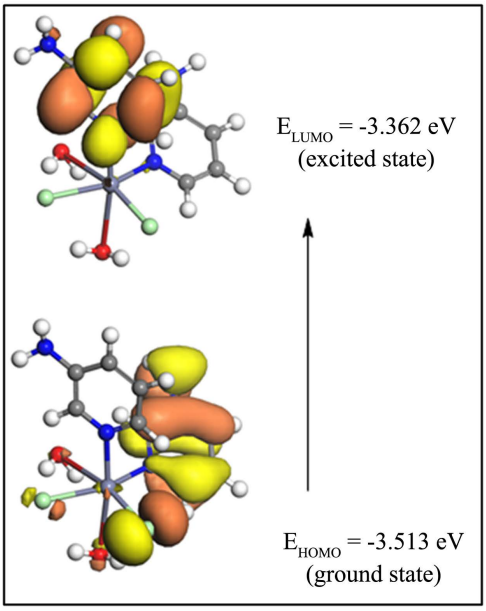

Figure 10. 3D plots frontier orbital energies of the complex $ZnCl_2$ ← 3-APy (1:2) using DFT method.

4. Conclusion

Seven Mn^{2+}, Co^{2+}, Ni^{2+}, Cu^{2+} and Zn^{2+}-3-aminopyridine (3-APy) complexes with variable stoichiometric ratios were prepared, characterized then, their antibacterial and cytotoxic activities toward some bacteria, fungi and human lung cancer were studied. The molecular structure of some selected metal complexes in view of chemical reactivity values such as chemical hardness, chemical potential electronegativity, electrophilicity index and HOMO-LUMO energy gap obtained theoretically were described. The latter data are used to understand their biological activities. The small HOMO-LUMO gap value and the chemical reactivity values show that the complexes are biologically active. It is worthy to mention that the experimental results belong to solid phase and theoretical calculations belong to gaseous phase. In the solid state, the existence of the crystal field along with the intermolecular interactions have connected the molecules together,

which result in the differences of bond parameters between the calculated and experimental values.

Conflicts of Interest

The authors declare no conflicts of interest regarding the publication of this paper.

References

[1] Altaf, A.A., Shahzad, A., Gul, Z., Rasool, N., Badshah, A., Lal, B. and Khan, E. (2015) A Review on the Medicinal Importance of Pyridine Derivatives. *Journal of Drug Design and Medicinal Chemistry*, **1**, 1-11. https://doi.org/10.1155/2015/913435

[2] Davood, A., Masoumeh, G., Mehdi, J., Roya, K., Mostafa, A. and Fatemeh, G. (2022) Green Synthesis and Biological Activities, Assessment of Some New Chromeno[2,3-b]pyridine Derivatives. *Molecular Diversity*, **26**, 891-902. https://doi.org/10.1007/s11030-021-10201-x

[3] Chavan, V., Sonawane, S., Shingare, M. and Karale, B. (2006) Synthesis, Characterization, and Biological Activities of Some 3,5,6-trichloropyridine Derivatives. *Chemistry of Heterocyclic Compounds*, **42**, 625-630. https://doi.org/10.1007/s10593-006-0137-8

[4] Sabet, R., Fassihi, A. and Moeinifard B. (2009) Preliminary MLR Studies of Antimicrobial Activity of Some 3-Hydroxypyridine-4-One and 3-Hydroxypyran-4-One Derivatives. *Research in Pharmaceutical Sciences*, **2**, 103-112. https://doi.org/10.3390/ijms9122407

[5] Abele, E., Abele, R. and Lukevics, E. (2003) Pyridine Oximes: Synthesis, Reactions, and Biological Activity. *Chemistry of Heterocyclic Compounds*, **39**, 825-865. https://doi.org/10.1023/A:1026181918567

[6] Bass, A.K.A., Abdelhafez, E.M.N., El-Zoghbi, M.S., *et al.* (2021) 3-Cyano-2-oxa-Pyridines: A Promising Template for Diverse Pharmacological Activities. *Journal of Advanced Biomedical and Pharmaceutical Sciences*, **4**, 81-86. https://doi.org/10.21608/jabps.2020.52641.1113

[7] Al-Fakeh, M.S., Allazzam, G.A. and Yarkandi, N.H. (2021) Ni(II), Cu(II), Mn(II), and Fe(II) Metal Complexes Containing 1,3-Bis(diphenylphosphino)propane and Pyridine Derivative: Synthesis, Characterization, and Antimicrobial Activity. *International Journal of Biomaterials*, **2021**, Article ID: 4981367. https://doi.org/10.1155/2021/4981367

[8] Ömer, Y., Dursun, A.K., Onur, Ş. and Demet, Ö. (2021) Mn(II) and Co(II) Mixed-Ligand Coordination Compounds with Acesulfame and 3-Aminopyridine: Synthesis and Structural Properties. *Journal of Coordination Chemistry*, **74**, 1168-1180. https://doi.org/10.1080/00958972.2021.1888083

[9] Zou, X.Z., *et al.* (2020) Pyridine Hydrazyl Thiazole Metal Complexes: Synthesis, Crystal Structure, Antibacterial and Antitumor Activity. *Inorganic Chemistry Communications*, **118**, Article ID: 108030. https://doi.org/10.1016/j.inoche.2020.108030

[10] Natalia, A., Francesca, V., Florencia, G., Gloria, S.M., Gabriela, K., Javier, E., Gianella, F., Laura, S. and María, H.T. (2020) New BI and TRI-Thiazole Copper(II) Complexes in the Search of New Cytotoxic Drugs against Breast Cancer Cells. *Inorganica Chimica Acta*, **508**, Article ID: 119622. https://doi.org/10.1016/j.ica.2020.119622

[11] Jungang D., Ping Y., Zhenlei Z., Jun W., Jinhua C., Na W., Hongbin S., Hong L., Feng Y. (2018) Designing Anticancer Copper(II) Complexes by Optimizing 2-Pyridine-Thiosemicarbazone Ligands. *European Journal of Medicinal Chemistry*, **158**, 442-452. https://doi.org/10.1016/j.ejmech.2018.09.020

[12] André, S.P., Cristiano, R.W.G. and Yifat, M. (2013) Molecular Modeling: Advancements and Applications. *Journal of Chemistry*, **2013**, Article ID: 875478.

[13] Kavitha, N. and Anantha, P.V.L. (2016) Synthesis, Characterization, Thermal and 3D Molecular Modeling Studies of Transition Metal Complexes Supported by ONN/ONO Tridentate Schiff Base Hydrazine. *Der Pharma Chemica*, **8**, 184-197. http://derpharmachemica.com/archive.html

[14] Parthiban, D., Baskaran, S., Rani, S., Arumugham, M.N., Si, N.T. and Kumar, R. (2021) Synthesis, Crystal Structure, DFT Analysis, and DNA Studies of a Binuclear Copper(II) Complex with 2,2'-Bipyridine and 4-Aminobenzoate. *Journal of Coordination Chemistry*, **74**, 2764-2779. https://doi.org/10.1080/00958972.2021.1985112

[15] Moustafa, M.E., Meshal, N.M., Ayad, M.I. and Goda, O.A. (2020) Aminopyridine Transition Metals Complexes, Characterization, Application and Molecular Orbital Calculation. *Benha Journal of Applied Sciences*, **35**, 231-243. https://doi.org/10.21608/bjas.2020.228550

[16] Parada, J. (2014) Synthesis Characterization and Antibacterial Activity of Cobalt(III) Complex with Phenanthroline and Maltose. *Journal of the Chilean Chemical Society*, **59**, 2636-2639. https://doi.org/10.4067/S0717-97072014000400002

[17] Schoenknecht, R.D. (1973) The Kirby-Bauer Technique in Clinical Medicine and Its Application to Carbenicillin. *The Journal of Infectious Diseases*, **127**, S111-S115. https://doi.org/10.1093/infdis/127.Supplement_2.S111

[18] Koch, W. and Holthausen, M.C.A. (2000) A Chemistry Guide to Density Functional Theory. Wiley-VCH, Weinheim.

[19] Parr, R.G. and Yang, W.T. (1989) Density Functional Theory of Atoms and Molecules. Oxford University Press, New York.

[20] (2011) In: Materials Studio. Accelrys Software Inc., San Diego.

[21] Patil, S., Unki, S., Kulkarni, A., Naik, V., Kamble, U. and Badami, P. (2011) Spectroscopic, *in Vitro* Antibacterial, and Antifungal Studies of Co(II), Ni(II), and Cu(II) Complexes with 4-Chloro-3-coumarinaldehyde Schiff Bases. *Journal of Coordination Chemistry*, **64**, 323-336. https://doi.org/10.1080/00958972.2010.541240

[22] Dharamraj, N., Viswanathamurthi, P. and Natrajan, K. (2001) Ruthenium(II) Complexes Containgbidentate Schiff Bases and Their Antifungal Activity. *Transition Metal Chemistry*, **26**, 105-109.

[23] Tweedy, B.G. (1964) Plant Extracts with Metal Ions as Potential Antimicrobial Agents. *Phytopathology*, **55**, 910-918.

[24] Yousef, T.A., El-Gammal, O.A., Ahmed, S.F. and El-Reash, G.M. (2015) Synthesis, Biological and Comparative DFT Studies on Ni(II) Complexes of NO and NOS Donor Ligands. *Spectrochimica Acta* (*A*): *Molecular and Biomolecular Spectroscopy*, **135**, 690-703. https://doi.org/10.1016/j.saa.2014.07.015

[25] Elamurugu, P.E. and Muthu, S. (2015) Vibrational Spectra, Molecular Structure, Natural Bond Orbital, First Order Hyperpolarizability, Thermodynamic Analysis and Normal Coordinate Analysis of Salicylaldehyde p-methylphenylthiosemicarbazone by Density Functional Method. *Spectrochimica Acta Part A*: *Molecular Spectroscopy*, **134**, 453-464. https://doi.org/10.1016/j.saa.2014.06.018

[26] Tanga, G.D., Zhao, J.Y., Li, R.Q., Cao, Y. and Zhang, Z.C. (2011) Synthesis, Charac-

teristic and Theoretical Investigation of the Structure, Electronic Properties and Second-Order Nonlinearity of Salicylaldehyde Schiff Base and Their Derivatives. *Spectrochimica Acta Part A*: *Molecular Spectroscopy*, **78**, 449-457.
https://doi.org/10.1016/j.saa.2010.11.008